

# Scaling properties of background- and chiral-magnetically-driven charge separation in heavy ion collisions at $\sqrt{s_{\text{NN}}} = 200$ GeV

Roy A. Lacey,<sup>1,\*</sup> Niseem Magdy,<sup>2</sup> Petr Parfenov,<sup>3</sup> and Arkadiy Taranenko<sup>3</sup>

<sup>1</sup>*Depts. of Chemistry & Physics, Stony Brook University, Stony Brook, New York 11794, USA*

<sup>2</sup>*Department of Physics, University of Illinois at Chicago, Chicago, Illinois 60607, USA*

<sup>3</sup>*National Research Nuclear University MEPhI, Moscow 115409, Russia*

(Dated: March 21, 2022)

The Anomalous Viscous Fluid Dynamics model, AVFD, is used in concert with the charge-sensitive correlator  $R_{\Psi_2}(\Delta S)$  to investigate the scaling properties of background- and chiral-magnetically-driven (CME) charge separation ( $\Delta S$ ), characterized by the inverse variance  $\sigma_{R_{\Psi_2}}^{-2}$  of the  $R_{\Psi_2}(\Delta S)$  distributions obtained in collisions at  $\sqrt{s_{\text{NN}}} = 200$  GeV. The  $\sigma_{R_{\Psi_2}}^{-2}$  values for the background are observed to be event-shape-independent. However, they scale with the reciprocal charged-particle multiplicity ( $1/\langle N_{\text{ch}} \rangle$ ), indicating an essential constraint for discerning background from the signal and a robust estimate of the difference between the backgrounds in Ru+Ru and Zr+Zr collisions. By contrast, the  $\sigma_{R_{\Psi_2}}^{-2}$  values for signal + background show characteristic  $1/\langle N_{\text{ch}} \rangle$  scaling violations that characterize the CME-driven contributions. Corrections to recent  $R_{\Psi_2}(\Delta S)$  measurements [1] that account for the background difference in Ru+Ru and Zr+Zr collisions indicate a charge separation difference compatible with the CME. The results further suggest that  $\sigma_{R_{\Psi_2}}^{-2}$  measurements for peripheral and central collisions in concert with  $1/\langle N_{\text{ch}} \rangle$  scaling, provides a robust constraint to quantify the background and aid characterization of the CME.

PACS numbers: 25.75.-q, 25.75.Gz, 25.75.Ld

Ion-ion collisions at the Relativistic Heavy Ion Collider (RHIC) and the Large Hadron Collider (LHC) lead to the production of a magnetized chiral relativistic quark-gluon plasma (QGP) [2–6], akin to the primordial plasma produced in the early Universe [7, 8] and several degenerate forms of matter found in compact stars [9]. Pseudo-relativistic analogs include Dirac and Weyl semimetals [10–12]. The study of anomalous transport in the QGP can give fundamental insight not only on the complex interplay of chiral symmetry restoration, axial anomaly and gluon topology [6, 13–16], but also on the evolution of magnetic fields in the early Universe [17, 18].

A major anomalous process predicted to occur in the magnetized QGP is the chiral magnetic effect (CME) [19]. It is characterized by the vector current:

$$\vec{J}_V = \frac{N_c e \vec{B}}{2\pi^2} \mu_A, \text{ for } \mu_A \neq 0, \quad (1)$$

where  $N_c$  is the color factor,  $\vec{B}$  is the magnetic field and  $\mu_A$  is the axial chemical potential that quantifies the axial charge asymmetry or imbalance between right- and left-handed quarks in the plasma [19–22]. Experimentally, the CME manifests as the separation of electrical charges along the  $\vec{B}$ -field [2, 19]. This stems from the fact that the CME preferentially drives charged particles, originating from the same “P-odd domain”, along or opposite to the  $\vec{B}$ -field depending on their charge.

The charge separation can be quantified via measurements of the first P-odd sine term  $a_1$ , in the Fourier decomposition of the charged-particle azimuthal distribution [23]:

bution [23]:

$$\frac{dN_{\text{ch}}}{d\phi} \propto 1 + 2 \sum_n (v_n \cos(n\Delta\phi) + a_n \sin(n\Delta\phi) + \dots) \quad (2)$$

where  $\Delta\phi = \phi - \Psi_{\text{RP}}$  gives the particle azimuthal angle with respect to the reaction plane (RP) angle, and  $v_n$  and  $a_n$  denote the coefficients of the P-even and P-odd Fourier terms, respectively. A direct measurement of the P-odd coefficients  $a_1$ , is not possible due to the strict global  $\mathcal{P}$  and  $\mathcal{CP}$  symmetry of QCD. However, their fluctuation and/or variance  $\tilde{a}_1 = \langle a_1^2 \rangle^{1/2}$  can be measured with charge-sensitive correlators such as the  $\gamma$ -correlator [23] and the  $R_{\Psi_2}(\Delta S)$  correlator [24–27].

The  $\gamma$ -correlator measures charge separation as:

$$\gamma_{\alpha\beta} = \langle \cos(\phi_\alpha + \phi_\beta - 2\Psi_2) \rangle, \quad \Delta\gamma = \gamma_{\text{OS}} - \gamma_{\text{SS}},$$

where  $\Psi_2$  is the azimuthal angle of the 2<sup>nd</sup>-order event plane which fluctuates about the RP,  $\phi$  denote the particle azimuthal emission angles,  $\alpha, \beta$  denote the electric charge (+) or (−) and SS and OS represent same-sign (++, --) and opposite-sign (+−) charges.

The  $R_{\Psi_2}(\Delta S)$  correlator [24, 25] measures charge separation relative to  $\Psi_2$  via the ratio:

$$R_{\Psi_2}(\Delta S) = C_{\Psi_2}(\Delta S) / C_{\Psi_2}^\perp(\Delta S), \quad (3)$$

where  $C_{\Psi_2}(\Delta S)$  and  $C_{\Psi_2}^\perp(\Delta S)$  are correlation functions that quantify charge separation  $\Delta S$ , approximately parallel and perpendicular (respectively) to the  $\vec{B}$ -field. The charge shuffling procedure employed in constructing these correlation functions ensures identical properties for their numerator and denominator, except for the

charge-dependent correlations, which are of interest [24, 25];  $C_{\Psi_2}(\Delta S)$  measures both CME- and background-driven charge separation while  $C_{\Psi_2}^{\perp}(\Delta S)$  measures only background-driven charge separation. The inverse variance  $\sigma_{R_{\Psi_2}}^{-2}$  of the  $R_{\Psi_2}(\Delta S)$  distributions serves to quantify the charge separation [24, 25, 28].

A vexing ongoing debate is whether the charge-sensitive  $R_{\Psi_2}(\Delta S)$  correlator [24–27] shows the requisite response and sensitivity necessary to (i) discern and characterize CME- and background-driven charge separation and (ii) pin down the influence of the background difference in collisions of Ru+Ru and Zr+Zr isobars. The latter is crucial for resolving the ambiguity reported for recent STAR measurements [1] which sought to determine a possible CME-driven charge separation difference for these isobars. Here, we employ the AVFD model [29, 30] to chart the  $R_{\Psi_2}(\Delta S)$  correlators’ response to varying degrees of signal and background, primarily in Au+Au collisions, to evaluate its efficacy for detecting and characterizing CME-driven charge separation in the presence of realistic backgrounds. We find characteristic scaling patterns for the background and scaling violations for signal + background that (i) discern between CME- and background-driven charge separation and (ii) allow a robust estimate of the background difference for the Ru+Ru and Zr+Zr isobars. Corrections to recent STAR  $R_{\Psi_2}(\Delta S)$  measurements [1], which accounts for this background difference, give results that suggest a CME-driven charge separation that is larger in Ru+Ru than in Zr+Zr collisions.

The AVFD model, which includes realistic estimates for charge-dependent backgrounds such as resonance decays and local charge conservation (LCC) is known to give good representations of the experimentally measured particle yields, spectra,  $v_n$ , etc [31]. Thus, it provides an essential benchmark for evaluating the interplay between possible CME- and background-driven charge separation in actual data. The model simulates charge separation resulting from the combined effects of the CME and the background. An in-depth account of its implementation can be found in Refs. [29] and [30]. In brief, the second-generation Event-by-Event version of the model, called E-by-E AVFD, uses Monte Carlo Glauber initial conditions to simulate the evolution of fermion currents in the QGP, in concert with the bulk fluid evolution implemented in the VISHNU hydrodynamic code [32], followed by a URQMD hadron cascade stage. Background-driven charge-dependent correlations result from LCC on the freeze-out hypersurface and resonance decays. A time-dependent magnetic field  $B(\tau) = \frac{B_0}{1+(\tau/\tau_B)^2}$ , acting in concert with a nonzero initial axial charge density  $n_5/s$ , is used to generate a CME current (embedded in the fluid dynamical equations), leading to a charge separation along the magnetic field. The peak values  $B_0$ , obtained from event-by-event simulations [33], are used

with a relatively conservative lifetime  $\tau_B = 0.6$  fm/c. The initial axial charge density, which results from gluonic topological charge fluctuations, is estimated based on the strong chromo-electromagnetic fields in the early-stage glasma. The present work uses the input scaling parameters for  $n_5/s$  and LCC to regulate the magnitude of the CME- and background-driven charge separation.

Simulated AVFD events were generated for varying degrees of signal and background for a broad set of centrality selections in Au+Au and isobar collisions for analysis with the  $R_{\Psi_2}(\Delta S)$  correlator. Here, it is noteworthy that the Monte Carlo Glauber parameters employed in the AVFD calculations for the isobars are similar to those used in the centrality calibrations reported in Ref. [1]; cross-checks ensured good agreement between the experimental and simulated  $N_{ch}$ -distributions for both isobars.

The event selection and cuts mimic those used in the analysis of experimental data [1]. Charged particles with transverse momentum  $0.2 < p_T < 2.0$  GeV/c are used to construct  $\Psi_2$ . Each event is subdivided into two sub-events with pseudorapidity  $0.1 < \eta < 1.0$  (E) and  $-1.0 < \eta < -0.1$  (W) to obtain  $\Psi_2^E$  and  $\Psi_2^W$  and their associated centrality-dependent event-plane resolution factors. The  $R_{\Psi_2}(\Delta S)$  distributions are determined for charged particles with  $0.35 < p_T < 2.0$  GeV/c, taking care to use  $\Psi_2^W$  for particles within the range  $0.1 < \eta < 1.0$  and  $\Psi_2^E$  for particles within the range  $-1.0 < \eta < -0.1$  to avoid possible self-correlations, as well as to reduce the influence of the charge-dependent non-flow correlations. The resulting distributions are corrected [ $R_{\Psi_2}(\Delta S'')$ ] to account for the effects of particle-number fluctuations and the event-plane resolution [24]. The sensitivity of  $R_{\Psi_2}(\Delta S)$  to variations in the elliptic flow ( $v_2$ ) magnitude at a selected centrality, is also studied using event-shape selection via fractional cuts on the distribution of the magnitude of the  $q_2$  flow vector [34]; for a given centrality, the magnitude of  $v_2$  is increased(decreased) by selecting events with larger(smaller)  $q_2$  magnitudes. This analysis aspect is performed with three sub-events ( $A[\eta < -0.3]$ ,  $B[|\eta| < 0.3]$ , and  $C[\eta > 0.3]$ ) using the procedures outlined earlier and  $q_2$  selection in sub-event  $B$ .

Figure 1 shows a representative comparison of the distributions obtained for signal (*Sig.*) + background (*Bkg.*) [ $n_5/s = 0.1$  and LCC=33%] and background without signal [LCC=33% and  $n_5/s = 0.0$ ] in 30-40% (a) and 60-70% (b) central Au+Au collisions. They show the expected concave-shaped distributions for background and signal + background respectively. For the 60-70% centrality cut, similar distributions are indicated for background and signal + background, suggesting a loss of sensitivity to the signal in these peripheral collisions. Such a loss will result if the  $\vec{B}$ -field is approximately randomly oriented to  $\Psi_2$  in these collisions. For the 30-40% centrality cut, Fig. 1 (a) shows a narrower distribution for signal + background than for background. This narrowing indicates that the CME signal increases the magnitude of

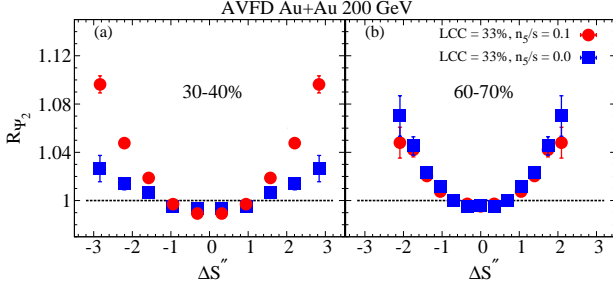


FIG. 1. Comparison of the  $R_{\Psi_2}(\Delta S)$  distributions for signal + background (solid circles) and background without signal (solid squares) for 30-40% (a) and 60-70% (b) Au+Au collisions at  $\sqrt{s_{NN}} = 200$  GeV.

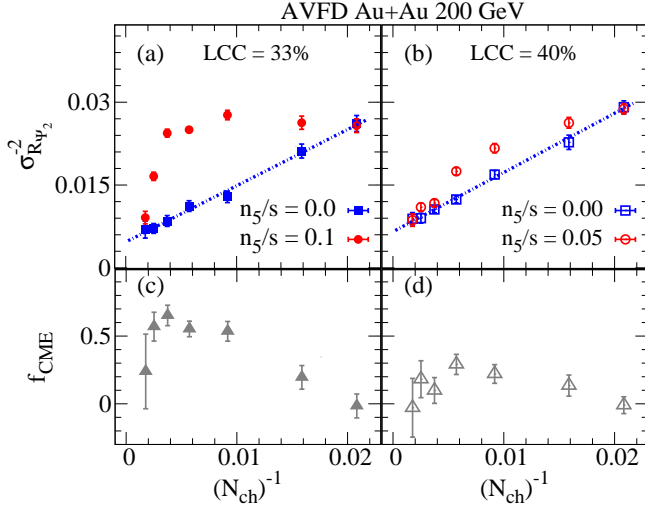


FIG. 2.  $\sigma_{R_{\Psi_2}}^{-2}$  vs.  $1/\langle N_{ch} \rangle$  [(a) and (b)] and  $f_{CME}$  vs.  $1/\langle N_{ch} \rangle$  [(c) and (d)] for Au+Au collisions at  $\sqrt{s_{NN}} = 200$  GeV, for two different parameter sets for signal and background as indicated. The dotted lines are drawn to guide the eye. The  $f_{CME}$  values in (c) and (d) characterize the fraction of the charge separation which is CME-driven following Eq. 4.

the charge separation beyond the level established by the background; this increase can be quantified via the fraction of the total charge separation attributable to the CME:

$$f_{CME} = \frac{[\sigma_{R_{\Psi_2}}^{-2}(Sig. + Bkg.) - \sigma_{R_{\Psi_2}}^{-2}(Bkg.)]}{[\sigma_{R_{\Psi_2}}^{-2}(Sig. + Bkg.)]}, \quad (4)$$

evaluated with the inverse variance ( $\sigma_{R_{\Psi_2}}^{-2}$ ) of the respective distributions. For the 30-40% central collisions shown in Fig. 1 (a),  $f_{CME} \approx 60\%$ . This value is a good benchmark of the sensitivity of the  $R_{\Psi_2}(\Delta S'')$  correlator to CME-driven charge separation of this level of signal ( $n_5/s = 0.1$ ) in the presence of charge-dependent background (LCC = 33%) in Au+Au collisions.

The centrality dependence of  $\sigma_{R_{\Psi_2}}^{-2}$  is summarized for

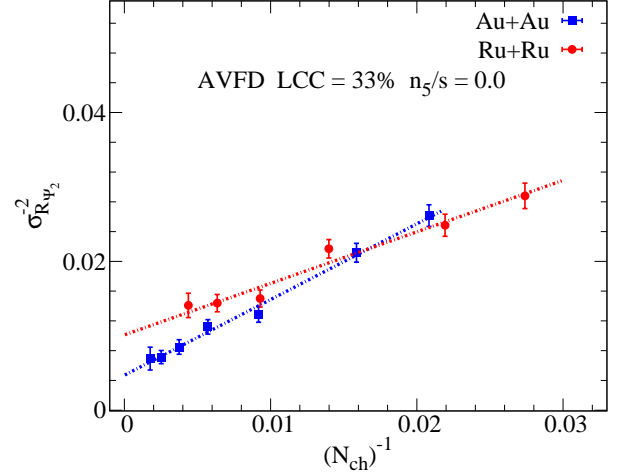


FIG. 3.  $\sigma_{R_{\Psi_2}}^{-2}$  vs.  $1/\langle N_{ch} \rangle$  for the background [LCC=33% and  $n_5/s = 0.0$ ] in Au+Au and Ru+Ru collisions at  $\sqrt{s_{NN}} = 200$  GeV. The dotted lines are drawn to guide the eye.

Au+Au collisions in Fig. 2 for two different parameter sets for signal and background as indicated. To highlight the scaling property of the background,  $\sigma_{R_{\Psi_2}}^{-2}$  is plotted vs.  $1/\langle N_{ch} \rangle$ , where  $\langle N_{ch} \rangle$  is the mean number of charged particles employed to evaluate  $R_{\Psi_2}(\Delta S)$  at the centrality of interest. Figs. 2 (a) and (b) show that the background scales as  $1/\langle N_{ch} \rangle$ , indicating that the observation of this scaling for the experimental  $\sigma_{R_{\Psi_2}}^{-2}$  measurements would be a strong indication for background-driven charge separation with very little if any, room for a CME contribution. Figs. 2 (a) and (b) also indicate comparable background and signal + background  $\sigma_{R_{\Psi_2}}^{-2}$  values for large and small  $\langle N_{ch} \rangle$ . This similarity suggests that background-driven charge separation dominates over the CME-driven contributions in the most central and peripheral collisions. Thus, the  $\sigma_{R_{\Psi_2}}^{-2}$  measurements for peripheral and central collisions can be leveraged with  $1/\langle N_{ch} \rangle$  scaling to give a quantitative estimate of the background over the entire centrality span.

The  $\sigma_{R_{\Psi_2}}^{-2}$  values, shown for signal + background in Figs. 2 (a), and (b), indicate characteristic positive deviations from the  $1/\langle N_{ch} \rangle$  scaling observed for the background. This apparent scaling violation gives a direct signature of the CME-driven contributions to the charge separation. They are quantified with the  $f_{CME}$  fractions (cf. Eq. 4) shown in Figs. 2 (c) and (d). The indicated  $f_{CME}$  values peak in mid-central collisions but reduce to zero at large and small  $\langle N_{ch} \rangle$ , i.e., central and peripheral collisions. They further indicate that, for these collisions, the  $R_{\Psi_2}(\Delta S'')$  correlator is sensitive to CME-driven charge separation even for a small signal ( $n_5/s = 0.05$ ) in the presence of significant charge-dependent background (LCC = 40%).

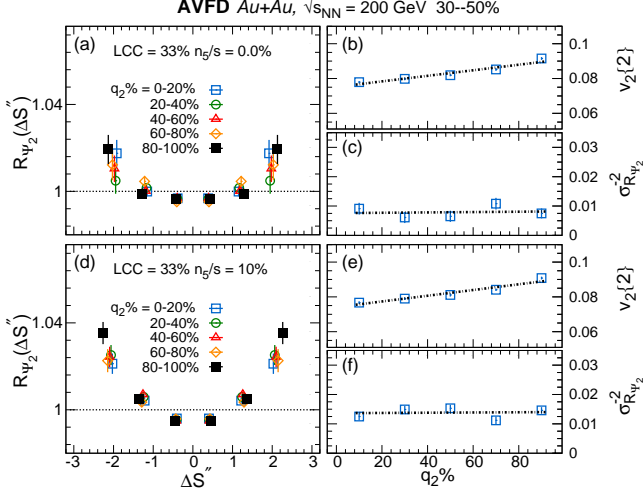


FIG. 4.  $q_2$  dependence of the  $R_{\Psi_2}(\Delta S'')$  distributions for background without signal [(a), (b) and (c)] and signal + background [(d), (e) and (f)]. The respective panels show the  $q_2$ -selected  $R_{\Psi_2}(\Delta S'')$  distributions [(a) and (d)], the corresponding  $v_2$  values [(b) and (e)], and the  $\sigma_{R_{\Psi_2}}^{-2}$  values [(c) and (f)] extracted from the distributions in (a) and (d).

The background  $\sigma_{R_{\Psi_2}}^{-2}$  values for Au+Au and Ru+Ru collisions are compared in Fig. 3. The results for Ru+Ru collisions show the same  $1/\langle N_{\text{ch}} \rangle$  scaling observed for Au+Au. However, they indicate that, for the same centrality, the  $\sigma_{R_{\Psi_2}}^{-2}$  values for Ru+Ru collisions are larger than those for Au+Au, suggesting a lowering of the sensitivity to the signal in collisions for the isobars.

The  $\sigma_{R_{\Psi_2}}^{-2}$  values extracted for background and signal + background at a given centrality, were checked to establish their sensitivity to variations in the magnitude of the anisotropic flow coefficient  $v_2$ . For this, as discussed earlier, event-shape selection via fractional cuts on the distribution of the magnitude of the  $q_2$  flow vector [34] was used. Representative results for the sensitivity of  $\sigma_{R_{\Psi_2}}^{-2}$  to a change in the magnitude of  $v_2$  [at a given centrality] are shown in Fig. 4 for background without signal [(a), (b) and (c)] and signal + background [(d), (e) and (f)] for Au+Au collisions. The respective panels show the  $q_2$ -selected  $R_{\Psi_2}(\Delta S'')$  distributions [(a) and (d)], the corresponding  $v_2$  values [(b) and (e)], and the  $\sigma_{R_{\Psi_2}}^{-2}$  values [(c) and (f)] extracted from the distributions shown in (a) and (d). They indicate that, while  $v_2$  shows a sizable increase with  $q_2$  (cf. panels (b) and (e)), the corresponding  $\sigma_{R_{\Psi_2}}^{-2}$  values (cf. panels (c) and (f)) are insensitive to  $q_2$  regardless of background or signal + background.

Similar patterns of insensitivity have been observed for the  $q_2$ -selected  $\sigma_{R_{\Psi_2}}^{-1}$  measurements reported for Ru+Ru and Zr+Zr collisions [1]. Notably, the reported insensitivity spans a  $\Delta v_2$  range (from low to high  $q_2$ ) much

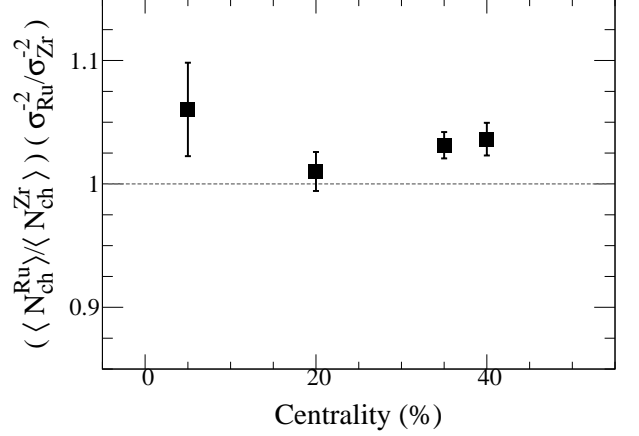


FIG. 5. Centrality dependence of the  $\langle N_{\text{ch}} \rangle$ -scaled ratio of the inverse variance of the  $R_{\Psi_2}(\Delta S'')$  distributions for Ru+Ru (Ru) and Zr+Zr (Zr) collisions at  $\sqrt{s_{\text{NN}}} = 200$  GeV.  $\langle N_{\text{ch}} \rangle$ -scaling corrects for the background difference between the two isobars.

larger than the measured difference between the  $v_2$  flow coefficients for the two isobars at a given centrality [1], indicating that the  $v_2$  difference between the isobars does not lead to an added difference in their  $\sigma_{R_{\Psi_2}}^{-2}$  values. Contributing factors to this insensitivity could stem from (i) an effective  $\Delta\eta$  gap between the event-plane and the interest particles that suppresses the charge-dependent non-flow correlations and (ii) the charge shuffling employed in the denominator of the correlation functions that comprise the  $R_{\Psi_2}(\Delta S'')$  correlator [24, 25]. The latter eliminates the charge-independent flow correlations and reduces the charge-dependent non-flow correlations.

The ratio of the inverse variance for the two isobars ( $\sigma_{\text{Ru+Ru}}^{-2} / \sigma_{\text{Zr+Zr}}^{-2}$ ) can also benchmark CME-driven charge separation, which is more prominent in collisions of Ru+Ru than Zr+Zr [1]. However, such a ratio must be corrected to account for the background difference between the two isobars. Since  $\sigma_{R_{\Psi_2}}^{-2}$  is  $q_2$ -independent and the background scales as  $1/\langle N_{\text{ch}} \rangle$ , a robust estimate for the correction factor at a given centrality is the ratio of the respective  $\langle N_{\text{ch}} \rangle$  values for the two isobars. The protocol for the STAR blind-analysis precluded the application of this correction to the  $R_{\Psi_2}(\Delta S'')$  measurements reported in Ref. [1], leading to an ambiguity in the interpretation of measurements that sought to determine a possible CME-driven charge separation difference between the two isobars. Fig. 5 shows the corrected ratios obtained using the  $\sigma_{\text{Ru+Ru}}^{-1} / \sigma_{\text{Zr+Zr}}^{-1}$  data reported for several centrality selections in Ref. [1]. The  $\langle N_{\text{ch}} \rangle$ -scaled ratios greater than 1.0 are consistent with more significant CME-driven charge separation in Ru+Ru collisions than Zr+Zr collisions.

In summary, AVFD model simulations that incorporate varying degrees of CME- and background-driven



charge separation are used to study the scaling properties of charge separation in heavy ion collisions at  $\sqrt{s_{NN}} = 200$  GeV. The inverse variance  $\sigma_{R_{\Psi_2}}^{-2}$  of the  $R_{\Psi_2}(\Delta S)$  distribution, that characterize the charge separation, indicate a linear dependence on  $1/\langle N_{ch} \rangle$  which is an essential constraint for discerning background from the signal and a precise estimate of the difference between the backgrounds in Ru+Ru and Zr+Zr collisions. By contrast, the  $\sigma_{R_{\Psi_2}}^{-2}$  values for signal + background show characteristic deviations from the  $1/\langle N_{ch} \rangle$  scaling, which serve to characterize the CME-driven contributions to the charge separation. Corrections to recent  $R_{\Psi_2}(\Delta S)$  measurements [1] that account for the background difference in Ru+Ru and Zr+Zr collisions, indicate a charge separation difference between the isobars compatible with the CME. The study further suggest that  $\sigma_{R_{\Psi_2}}^{-2}$  measurements for peripheral and central collisions can be leveraged with  $1/\langle N_{ch} \rangle$  scaling to quantify the background and aid characterization of the CME in a wealth of available systems.

## ACKNOWLEDGMENTS

This research is supported by the US Department of Energy, Office of Science, Office of Nuclear Physics, under contracts DE-FG02-87ER40331.A008 (RL) and DE-FG02-94ER40865 (NM).

---

\* Roy.Lacey@stonybrook.edu

- [1] Mohamed Abdallah *et al.* (STAR), “Search for the chiral magnetic effect with isobar collisions at  $\sqrt{s_{NN}}=200$  GeV by the STAR Collaboration at the BNL Relativistic Heavy Ion Collider,” *Phys. Rev. C* **105**, 014901 (2022), arXiv:2109.00131 [nucl-ex].
- [2] Dmitri Kharzeev, “Parity violation in hot QCD: Why it can happen, and how to look for it,” *Phys. Lett. B* **633**, 260–264 (2006), arXiv:hep-ph/0406125.
- [3] Jinfeng Liao, “Anomalous transport effects and possible environmental symmetry ‘violation’ in heavy-ion collisions,” *Pramana* **84**, 901–926 (2015), arXiv:1401.2500 [hep-ph].
- [4] Vladimir A. Miransky and Igor A. Shovkovy, “Quantum field theory in a magnetic field: From quantum chromodynamics to graphene and Dirac semimetals,” *Phys. Rept.* **576**, 1–209 (2015), arXiv:1503.00732 [hep-ph].
- [5] Xu-Guang Huang, “Electromagnetic fields and anomalous transports in heavy-ion collisions — A pedagogical review,” *Rept. Prog. Phys.* **79**, 076302 (2016), arXiv:1509.04073 [nucl-th].
- [6] D. E. Kharzeev, J. Liao, S. A. Voloshin, and G. Wang, “Chiral magnetic and vortical effects in high-energy nuclear collisions—A status report,” *Prog. Part. Nucl. Phys.* **88**, 1–28 (2016), arXiv:1511.04050 [hep-ph].
- [7] Igor Rogachevskii, Oleg Ruchayskiy, Alexey Boyarsky, Jürg Fröhlich, Nathan Kleeorin, Axel Brandenburg, and Jennifer Schober, “Laminar and turbulent dynamos in chiral magnetohydrodynamics-I: Theory,” *Astrophys. J.* **846**, 153 (2017), arXiv:1705.00378 [physics.plasm-ph].
- [8] Valery A. Rubakov and Dmitry S. Gorbunov, *Introduction to the Theory of the Early Universe* (World Scientific, Singapore, 2017).
- [9] Fridolin Weber, “Strange quark matter and compact stars,” *Prog. Part. Nucl. Phys.* **54**, 193–288 (2005), arXiv:astro-ph/0407155 [astro-ph].
- [10] Oskar Vafek and Ashvin Vishwanath, “Dirac Fermions in Solids: From High-Tc cuprates and Graphene to Topological Insulators and Weyl Semimetals,” *Ann. Rev. Condensed Matter Phys.* **5**, 83–112 (2014), arXiv:1306.2272 [cond-mat.mes-hall].
- [11] A. A. Burkov, “Chiral anomaly and transport in Weyl metals,” *J. Phys. Condens. Matter* **27**, 113201 (2015), arXiv:1502.07609 [cond-mat.mes-hall].
- [12] E. V. Gorbar, V. A. Miransky, I. A. Shovkovy, and P. O. Sukhachov, “Anomalous transport properties of Dirac and Weyl semimetals (Review Article),” *Low Temp. Phys.* **44**, 487–505 (2018), [Fiz. Nizk. Temp. **44**, 635 (2017)], arXiv:1712.08947 [cond-mat.mes-hall].
- [13] Guy D. Moore and Marcus Tassler, “The Sphaleron Rate in SU(N) Gauge Theory,” *JHEP* **02**, 105 (2011), arXiv:1011.1167 [hep-ph].
- [14] M. Mace, S. Schlichting, and R. Venugopalan, “Off-equilibrium sphaleron transitions in the Glasma,” *Phys. Rev. D* **93**, 074036 (2016), arXiv:1601.07342 [hep-ph].
- [15] Jinfeng Liao, Volker Koch, and Adam Bzdak, “On the Charge Separation Effect in Relativistic Heavy Ion Collisions,” *Phys. Rev. C* **82**, 054902 (2010), arXiv:1005.5380 [nucl-th].
- [16] Volker Koch, Soeren Schlichting, Vladimir Skokov, Paul Sorensen, Jim Thomas, Sergei Voloshin, Gang Wang, and Ho-Ung Yee, “Status of the chiral magnetic effect and collisions of isobars,” *Chin. Phys. C* **41**, 072001 (2017), arXiv:1608.00982 [nucl-th].
- [17] M. Joyce and Mikhail E. Shaposhnikov, “Primordial magnetic fields, right-handed electrons, and the Abelian anomaly,” *Phys. Rev. Lett.* **79**, 1193–1196 (1997), arXiv:astro-ph/9703005 [astro-ph].
- [18] Hiroyuki Tashiro, Tanmay Vachaspati, and Alexander Vilenkin, “Chiral Effects and Cosmic Magnetic Fields,” *Phys. Rev. D* **86**, 105033 (2012), arXiv:1206.5549 [astro-ph.CO].
- [19] Kenji Fukushima, Dmitri E. Kharzeev, and Harmen J. Warringa, “The Chiral Magnetic Effect,” *Phys. Rev. D* **78**, 074033 (2008), arXiv:0808.3382 [hep-ph].
- [20] Dam T. Son and Piotr Surowka, “Hydrodynamics with Triangle Anomalies,” *Phys. Rev. Lett.* **103**, 191601 (2009), arXiv:0906.5044 [hep-th].
- [21] Valentin I. Zakharov, “Chiral Magnetic Effect in Hydrodynamic Approximation,” (2012), 10.1007/978-3-642-37305-3-11, [Lect. Notes Phys. **871**, 295 (2013)], arXiv:1210.2186 [hep-ph].

- [22] Kenji Fukushima, “Views of the Chiral Magnetic Effect,” *Lect. Notes Phys.* **871**, 241–259 (2013), arXiv:1209.5064 [hep-ph].
- [23] Sergei A. Voloshin, “Parity violation in hot QCD: How to detect it,” *Phys. Rev.* **C70**, 057901 (2004), arXiv:hep-ph/0406311 [hep-ph].
- [24] Niseem Magdy, Shuzhe Shi, Jinfeng Liao, N. Ajitanand, and Roy A. Lacey, “A New Correlator to Detect and Characterize the Chiral Magnetic Effect,” (2017), arXiv:1710.01717 [physics.data-an].
- [25] Niseem Magdy, Shuzhe Shi, Jinfeng Liao, Peifeng Liu, and Roy A. Lacey, “Examination of the observability of a chiral magnetically driven charge-separation difference in collisions of the  $^{96}_{44}\text{Ru} + ^{96}_{44}\text{Ru}$  and  $^{96}_{40}\text{Zr} + ^{96}_{40}\text{Zr}$  isobars at energies available at the BNL Relativistic Heavy Ion Collider,” *Phys. Rev.* **C98**, 061902 (2018), arXiv:1803.02416 [nucl-ex].
- [26] Ling Huang, Mao-Wu Nie, and Guo-Liang Ma, “Sensitivity analysis of the chiral magnetic effect observables using a multiphase transport model,” (2019), arXiv:1906.11631 [nucl-th].
- [27] Niseem Magdy, Mao-Wu Nie, Guo-Liang Ma, and Roy A. Lacey, “A sensitivity study of the primary correlators used to characterize chiral-magnetically-driven charge separation,” (2020), arXiv:2002.07934 [nucl-ex].
- [28] Shuzhe Shi, Hui Zhang, Defu Hou, and Jinfeng Liao, “Signatures of Chiral Magnetic Effect in the Collisions of Isobars,” *Phys. Rev. Lett.* **125**, 242301 (2020), arXiv:1910.14010 [nucl-th].
- [29] Shuzhe Shi, Yin Jiang, Elias Lilleskov, and Jinfeng Liao, “Anomalous Chiral Transport in Heavy Ion Collisions from Anomalous-Viscous Fluid Dynamics,” *Annals Phys.* **394**, 50–72 (2018), arXiv:1711.02496 [nucl-th].
- [30] Yin Jiang, Shuzhe Shi, Yi Yin, and Jinfeng Liao, “Quantifying the chiral magnetic effect from anomalous-viscous fluid dynamics,” *Chin. Phys.* **C42**, 011001 (2018), arXiv:1611.04586 [nucl-th].
- [31] Ulrich Heinz, Olga Evdokimov, and Peter Jacobs, eds., *Proceedings, 26th International Conference on Ultra-relativistic Nucleus-Nucleus Collisions (Quark Matter 2017): Chicago, Illinois, USA, February 5-11, 2017*, Vol. 967 (Elsevier, 2017).
- [32] Chun Shen, Zhi Qiu, Huichao Song, Jonah Bernhard, Steffen Bass, and Ulrich Heinz, “The iEBE-VISHNU code package for relativistic heavy-ion collisions,” *Comput. Phys. Commun.* **199**, 61–85 (2016), arXiv:1409.8164 [nucl-th].
- [33] John Bloczynski, Xu-Guang Huang, Xilin Zhang, and Jinfeng Liao, “Azimuthally fluctuating magnetic field and its impacts on observables in heavy-ion collisions,” *Phys. Lett. B* **718**, 1529–1535 (2013), arXiv:1209.6594 [nucl-th].
- [34] Jurgen Schukraft, Anthony Timmins, and Sergei A. Voloshin, “Ultra-relativistic nuclear collisions: event shape engineering,” *Phys. Lett. B* **719**, 394–398 (2013), arXiv:1208.4563 [nucl-ex].
- [35] “Charge separation measurements in  $p(d)+\text{Au}$  and  $\text{Au}+\text{Au}$  collisions; implications for the chiral magnetic effect,” (2020), Note that the error recently found in the evaluation of  $R_{\Psi_3}(\Delta S)$  has no impact on the  $R_{\Psi_2}(\Delta S)$  data reported in [35] and employed in the present study., arXiv:2006.04251.